Separation and Purification Technology 359 (2025) 130445

Contents lists available at ScienceDirect

Separation and Purification Technology

journal homepage: www.elsevier.com/locate/seppur

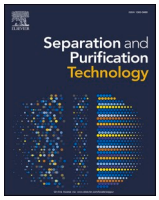

Modeling and estimation of CO_2 capture by porous liquids through machine learning

Farid Amirkhani [a], Amir Dashti [a], Hossein Abedsoltan [b,c], Amir H. Mohammadi [d,e,*], John L. Zhou [a,*], Ali Altaee [a]

[a] Centre for Green Technology, School of Civil and Environmental Engineering, University of Technology Sydney, Sydney, NSW 2007, Australia
[b] Department of Chemical Engineering, University of Toledo, Toledo, OH, USA
[c] Linda and Bipin Doshi Department of Chemical and Biochemical Engineering, Missouri University of Science and Technology, Rolla, Missouri, 65401, USA
[d] Institut de Recherche en Génie Chimique et Pétrolier (IRGCP), Paris Cedex, France
[e] Discipline of Chemical Engineering, School of Engineering, University of KwaZulu-Natal, Howard College Campus, King George V Avenue, Durban 4041, South Africa

ARTICLE INFO

Editor: S Yi

Keywords:
CO_2 absorption
Greenhouse gas
Machine learning
Modeling
Porous liquids

ABSTRACT

Porous liquids (PLs) are newly developed porous materials that combine unique fluidity with permanent porosity, which exhibit promising functionalities. They have shown ability to efficiently absorb greenhouse gases such as carbon dioxide (CO_2). Experimental measurement is one approach to determining the solubility of various greenhouse gases in PLs, which has drawbacks such as being expensive and time-consuming. Hence, simulation models are valuable to predict the solubility of CO_2 in various PLs. This work aims to develop machine learning (ML) modeling methods for accurately estimating CO_2 solubility under varying conditions (e.g. PLs, temperature, pressure). Adaptive Neuro-Fuzzy Inference System (ANFIS), Particle Swarm Optimization-ANFIS (PSO-ANFIS), Coupled Simulated Annealing-Least Squares Support Vector Machine (CSA-LSSVM), and Multilayer Perceptron Neural Network (MLP-NN) were established as the state of art algorithms for estimating CO_2 solubility. The models demonstrated accurate modeling results with average absolute relative deviation (AARD) of 12.98%, 8.67%, 3.17% and 6.64% for ANFIS, PSO-ANFIS, CSA-LSSVM and MLP-NN, respectively. This work has presented a powerful modeling tool with few parameters that need to be controlled, to precisely estimate CO_2 solubility in different PLs of complex structures.

1. Introduction

The swift advancement of human civilization since the Industrial Revolution has resulted in a notable surge in the global energy consumption rate, reaching 15 terawatts (TW) in 2010 and is projected to climb to 27 TW by 2050 [1]. Conversely, our primary energy requirements continue to be met by finite and nonrenewable fossil fuels, such as coal, petroleum, and natural gas [2]. Excessive dependence on these fossil fuels has not only contributed to air and water pollution, but also triggered a substantial escalation in CO_2 emissions into the atmosphere, leading to severe global alterations in climate and causing detrimental impacts on the environment [3]. In 2020, CO_2 emissions stemming from the combustion of fossil fuels amounted to 34 billion tons and were anticipated to increase further [4]. The repercussions of the greenhouse effect are evident in global climate change, manifesting as phenomena like global warming, rising sea levels, and the melting of glaciers, posing a threat to the survival of humanity. The Intergovernmental Panel on Climate Change (IPCC) has proposed the restriction of the global average temperature rise to 1.5 ℃ within the next century as a long-term objective [5]. The most favorable approach for mitigating CO_2 emissions in power plants is considered to be post combustion capture technology, which has already found application in the electricity industry [6]. Out of the four post combustion methods, namely adsorption [7], absorption [8], membrane separation [9–11], and cryogenic separation [12], absorption is regarded as the most viable option for large-scale implementation in CO_2 capture. This preference is attributed to its notable CO_2 capture efficiency and exceptional adaptability within existing power plants [13].

In absorption processes, alkanolamine aqueous solutions, specifically monoethanolamine, serve as the absorbents. Despite their exceptional efficiency in CO_2 separation, these solutions have certain drawbacks, including high consumption of renewable energy,

* Corresponding authors.
E-mail addresses: amir_h_mohammadi@yahoo.com (A.H. Mohammadi), junliang.zhou@uts.edu.au (J.L. Zhou).

https://doi.org/10.1016/j.seppur.2024.130445
Received 30 July 2024; Received in revised form 5 November 2024; Accepted 6 November 2024
Available online 8 November 2024

susceptibility to corrosion, and decomposition issues [14]. As a promising alternative, porous liquids (PLs) emerge as novel absorbents that combine the fluid characteristics of liquids with the porous nature of solid materials. Consequently, PLs are considered a favorable option for CO_2 capture. Unlike traditional absorbents [15], PLs boast abundant pores, providing additional adsorption sites for CO_2 and thereby enhancing the overall CO_2 absorption capacity. In the realm of gas separation, PLs offer distinct advantages compared to solid adsorbents due to their liquid state, making them suitable for use in continuous separation processes based on solvents. Moreover, they exhibit advantages over traditional liquid absorbents because the pores within PLs can be specifically designed to match the size and shape of the target gas. This tailored design capability enhances the selectivity of the target gas in mixed gas scenarios, resulting in increased effectiveness [16]. As a result, PLs exhibit numerous advantages over their traditional solid or liquid counterparts [17]. The fluidic nature of PLs enables easy integration into existing continuous flow liquid-based separation processes. Furthermore, their inherent permanent porosity enhances gas capture with selectivity based on size and shape [18], showcasing considerable potential for applications in gas adsorption, separation, and catalysis [19].

So far, the primary applications of PLs have targeted gas adsorption. Consequently, earlier PLs were largely engineered for capturing gases such as CO_2, CH_4, and others [20]. For instance, Dai et al. primarily focused on CO_2 adsorption using PLs [21]. Xin et al. [22] proposed a versatile and straightforward method for synthesizing type III PLs with reduced viscosity, following the principle of "like dissolves like." A recent investigation by Gomes et al. [23] might offer novel insights for the development of high-efficiency PLs for CO_2 capture under low pressure. Specifically, PLs incorporating ZIF-8 and phosphonium acetate or levulinate salts exhibit CO_2 adsorption at low pressure, achieving a capacity of 1.5 mmol g^{-1} at 303 K and 2 bar. This is comparable to the performance of popular sorbent materials, such as ethanolamines (1.8 mmol g^{-1} for N-methyl-diethanolamine at 40 °C and 1 bar) or solid amine sorbents (2.6 mmol g^{-1} for mesoporous silica functionalized with polyethyleneimine at 30 °C and 1 bar) [24]. Therefore, such research strengthens our belief that PLs could offer an enhanced solution for gas adsorption at low pressure with optimized designs.

Due to the difficulties involved in experimental measurements, given their time-consuming and expensive nature, the development of predictive methods to estimate the phase behavior of such systems is highly beneficial to support UN Sustainable Development Goals. Additionally, for the efficient design of processes dealing with mixtures of CO_2 in ionic liquids, it is crucial to determine the operational conditions required to attain a desired level of CO_2 solubility in the chosen ionic liquid solvent [25]. To investigate the application of ML techniques in CO_2 capture processes, RBFNN, SVR, and XGBoost models were used for computing the equilibrium solubility of CO_2 in blended amine solutions containing MEA-DEEA and MEA-MDEA [26]. Modeling techniques have also been suggested for CO_2/PLs systems to calculate CO_2 solubility.

Mukesh et al. [27] used the Redlich-Kwong cubic type EOS to estimate the solubility behavior of CO_2 in a porous ionic liquid (type-III). Atilhan et al. [28] used molecular simulation tools to investigate nanoscopic interactions CO_2 capture in porous liquids. Quantum chemistry calculations using Density Functional Theory were used in their study. However, these models lack generality, and therefore there is a need to develop models that can be applied to estimate phase behaviors such as solubility in a wide range of CO_2/PLs conditions [29].

Nevertheless, it is essential to consider that, for example, ionic liquid molecules consist of highly asymmetric neutral ion pairs characterized by a substantial dipole moment resulting from the charge distribution across the ion pair [30]. Additionally, given the quadrupole moment of CO_2 molecules [30], any applied thermodynamic relations must be capable of accommodating these intense interactions. Moreover, it is crucial to account for the effects of elevated pressures commonly encountered in supercritical operations. The existing thermodynamic models mentioned earlier have primarily been tailored for specific systems due to these two factors, rather than applying to a range of systems with general applicability. Consequently, there arises a necessity to formulate general models capable of predicting the phase behaviors of diverse systems involving various types of ionic liquids, which are now being considered alternatives to conventional industrial solvents [25].

There are several studies on topics related to CO_2 by utilizing ML techniques [31]. Some of these studies propose methods to predict CO_2 solubility in different solvents. For instance, artificial neural network (ANN) was used to predict CO_2 solubility at equilibrium conditions in propanol-based solvents [32]. Another example relates to the estimations of CO_2 solubility in amine solutions, using ANN and ANFIS [33]. For eutectic mixtures, ANFIS and gene expression programming (GEP) were used as ML techniques [34]. The least square support vector machine (LSSVM) is also reported as a ML technique to predict CO_2 solubility [35]. However, there is a lack of systematic comparison between different ML models in their performance of modeling CO_2 solubility in PLs.

As PLs can be complex chemicals, traditional modeling of CO_2 solubility in PLs, such as thermodynamic models, can be highly complicated, new ML models and methodology for input selection are proposed in this study. Therefore, the objectives of this study were to develop four ML modeling methods (ANFIS, PSO-ANFIS, CSA-LSSVM, MLP-NN) in estimating CO_2 solubility in a diverse range of PLs; to assess the performance of the different models by comparing predicted vs actual CO_2 solubility results in PLs; and to conduct statistical analysis of the modeling results.

2. Theory of machine learning models

2.1. Adaptive neuro-fuzzy inference system (ANFIS)

ANFIS is a common model do for estimations in petroleum and chemical engineering. This model was first proposed with five combined algorithms to modify the fuzzy system and neural network [36–38]. Hybrid learning algorithms and back propagation method are usually used to train the ANFIS topology [39]. An ANFIS with two inputs and one output will have a mathematical formula (equation (1)) for a specific node I in the first layer [36]:

$$O_i^1 = \mu_{A_i}(x) \tag{1}$$

where x, O_i^1, μ_{A_i} are the input, output of the node, membership function associated with the linguistic label A_i, respectively. Each node has value in the range of 0 to 1 where membership function (MF) can define it. In this study, Gaussian type was used as the MF, defined by equation (2) [40]:

$$\mu_A(\mathrm{x}) = e^{-\frac{(x-Z)^2}{2\sigma^2}} \tag{2}$$

where Z is the center of Gaussian MF, and σ^2 represents the variance parameter. For the second layer, two other parameters of constant nodes and some weighted terms will be added and the correlation will be as shown in equation (3) [41]:

$$O_i^2 = \omega_i = \mu_{A_i}(x)\mu_{B_i}(y) \tag{3}$$

where ω_i represents the firing strength or weight of the i-th rule in the system. O denotes the output of layer, which can calculate the mean value for weighted terms, which is then applied in the third layer by equation (4) [42]:

$$O_i^3 = \overline{\omega}_i = \frac{\omega_i}{\omega_1 + \omega_2} \tag{4}$$

Multiplication of each average weight by its corresponding function is completed for the fourth layer by equation (5) [42]:

$$O_i^4 = \overline{\omega}_i f_i = \overline{\omega}_i (p_i x + q_i y + r_i) \quad (5)$$

where r_i, q_i and p_i are the resulting and tunable parameters. The final value will be obtained by adding up all the stated outputs in the fifth layer by equation (6) [42]:

$$O_i^5 = \sum_i \overline{\omega}_i f_i = \frac{\sum_i \omega_i f_i}{\sum_i \omega_i} \quad (6)$$

The schematic diagram of an ANFIS structure is shown in Fig. 1.

2.1.1. PSO

PSO is an algorithm to optimize the outputs stochastically. Its concept is formed on the based on how the group-living animals communicate and relocate [44]. The PSO has a searching process that firstly creates a population called a swarm- having separate parts as individuals that express particles. The corresponding positions determine possible resolutions to find an optimized solution for the problem. Every particle has a velocity which is a defining parameter for the particle during the searching process. In this work, the parameters of ANFIS were optimized by applying PSO [45–48].

2.2. CSA-LSSVM

The Support Vector Machine (SVM), initially introduced by Vapnik [49], is a pivotal ML method utilized for classifying or predicting target data within nonlinear systems [50]. Another formulation for SVM, known as the Least Squares Support Vector Machine (LSSVM), was developed [51]. LSSVM presents several advantageous features compared to SVM, including faster convergence, simpler calculations, and higher accuracy [51]. In LSSVM, the approach involves predicting an approximation function through the utilization of training data.

A dataset consisting of $(x_i, y_i)_n$ is considered, where x_i, y_i and n represent the input points, target points, and the total number of training data points, respectively. The LSSVM regression approach is applied to estimate any arbitrary function. This linear regression model is expressed as equation (7) [52]:

$$f(x) = \omega^T \varphi + b \quad (7)$$

where φ denotes nonlinear function where as ω shows weight vector and b is considered a constant term. To approximate the function, equations (8) and (9) are utilized [53]:

$$min_{\omega,\, b,\, e} J(\omega,\, e) = \frac{1}{2}\|\omega\|^2 + \frac{1}{2}\gamma \sum_{i=1}^{n} e_i^2 \quad (8)$$

$$y_i = \langle \omega,\, \varphi(x_i) \rangle + b + e_i \quad (9)$$

where e_i and γ indicate error and regularization variables, respectively.

To formulate the optimization problem, the Lagrangian function (equation (10) is constructed [54]:

$$L_{lssvm} = \frac{1}{2}\|w\|^2 + \frac{1}{2}\gamma \sum_{i=1}^{N} e_i^2 - \sum_{k=1}^{N} \alpha_k \{(\omega.\varphi(x_k)) + b + e_k - y_k\} \quad (10)$$

where α_k denotes the Lagrange multiplier. The optimization process is solved based on partial differential concept [55]:

$$\frac{\partial L_{LSSVM}}{\partial_w} = 0 \rightarrow w = \sum_{k=1}^{N} \alpha_k \varphi(x_k) \quad (11)$$

$$\frac{\partial L_{LSSVM}}{\partial_b} = 0 \rightarrow \sum_{k=1}^{N} \alpha_k = 0 \quad (12)$$

$$\frac{\partial L_{LSSVM}}{\partial_{e_k}} = 0 \rightarrow \alpha_k = \gamma e_k \;\; k = 1, \cdots, N \quad (13)$$

$$\frac{\partial L_{LSSVM}}{\partial_{\alpha_k}} = 0 \rightarrow (w.\varphi(x_k)) + b + e_k - y_k = 0 \;\; k = 1, \cdots, N \quad (14)$$

where $\alpha = [\alpha_1, \cdots, \alpha_N]$, $l_v = [1, \cdots 1]$, $Y = [y_1, \cdots y_N]$, and ω and e_k are excluded to form equation (15):

$$\begin{bmatrix} 0 & I_N^T \\ I_N & \Omega + \gamma^{-1} I_N \end{bmatrix} \begin{bmatrix} b \\ \alpha \end{bmatrix} = \begin{bmatrix} 0 \\ Y \end{bmatrix} \quad (15)$$

where Ω and I_N present the kernel and identity matrices, respectively. The kernel function is outlined in equation (16):

$$\Omega_{ij} = \varphi(x_i)\varphi(x_j) = K(x_i,\, x_j) \quad (16)$$

The LSSVM methodology incorporates various types of kernel functions, including the radial basis function, which is defined as follows:

$$K(x_i, x_j) = e^{\left(\frac{\|x_i - x_j\|^2}{\sigma^2}\right)} \quad (17)$$

Simulated annealing (SA) stands as a versatile optimization technique, drawing inspiration from the annealing process in solids. It was initially proposed by Kirkpatrick et al. [56] to tackle intricate modeling tasks. The primary objective of this method is to address limitations present in other optimization approaches, including the risk of being confined to local minima, non-differentiability of cost functions, and high computational expenses. To refine the SA approach, [57] introduced a collection of techniques for globally optimizing continuous parameters, termed CSA. CSA ensures superior optimization capabilities compared to standalone SA approaches by creating a hybrid system that exchanges information to decide whether an uphill movement should be considered [58]. CSA-LSSVM have been used in many other regressions and prediction-based research [59–64].

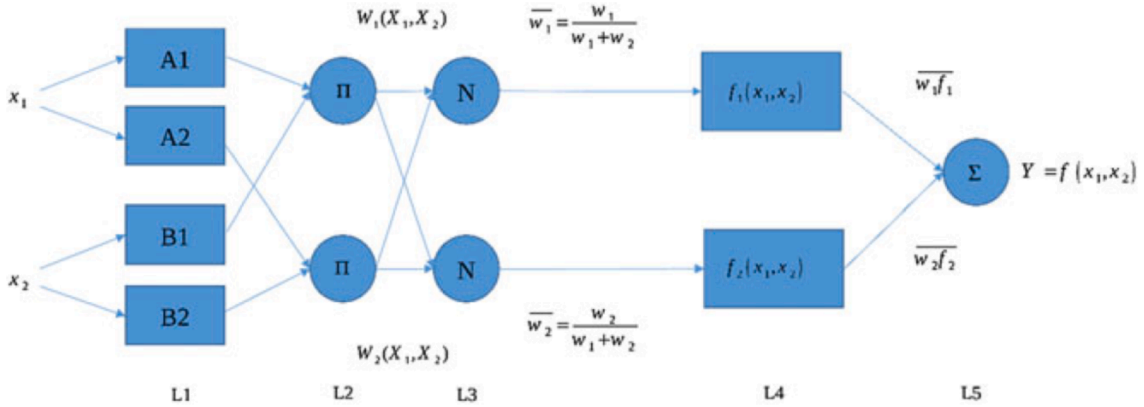

Fig. 1. Structure of ANFIS model with two input parameters [43]. Copyright 2017, Reproduced with permission from Wiley.

Given the significant applicability of CSA [64], this study employs CSA, utilizing σ^2 and γ as optimization variables to determine the optimal configuration of the LSSVM model's tuning parameters. Fig. 2 shows the schematic of CSA-LSSVM algorithm.

2.3. MLP-NN

ANNs were developed based on the human nervous system, and have been used for regression analysis, function estimation, pattern identification, and classification of problems. The ANN can mainly find a relation between input and output problems by attributing a function. The ANN has processing and interconnecting parts, known as weights and nodes, respectively [66]. Two famous ANNs are RBF and MLP. Neuron's information processing is an approach to distinguish RBF from MLP. For RBF modeling, no connection between the input layers and the hidden ones is assumed. For MLP modeling, there is a relation between the hidden and the output layers. The number of neurons in output and hidden layers corresponds to unity and number of input parameters. The hidden layer specifies the function connecting the input variables and the output of the model [67].

ANNs are composed of synthetic neurons that function as basic processing units. Independent variables, serving as input variables, are introduced to the input layer and subsequently passed to the artificial neurons within the hidden layers, before finally reaching the output layer in sequence. A schematic illustration of the ANN structure is shown in Fig. 3 [68].

The strengths or weaknesses of connections between inputs and neurons are determined by the weight parameters. In this study, a feed-forward neural network (FNN) model with a modified Levenberg–Marquardt optimization algorithm is employed for training. To generate the inputs along with their associated weight coefficients, biases are incorporated. The neuron's output is determined using equation (18) [68]:

$$n_j = f\left(\sum_{r=1}^{N} w_{jr}x_r + b_j\right) \tag{18}$$

where n_j denotes the neuron output. The function f serves as a transfer function through which the net output of each neuron is processed. w_{jr} is a weight coefficient, x_r is an input, and b_j is a bias [68].

In this study, the logarithmic sigmoid function is utilized as the transfer function, defined in equation (19) [69]:

$$f(x) = \frac{1}{1+\exp(-x)} \tag{19}$$

3. Data collection for CO_2 absorption in PLs

The experimental data for CO_2 absorption in PLs was obtained from literature search using the web of science. A range of diverse PLs were studied in this work including ZIF-8/[DBU-PEG]-[NTf_2], ZSM-5/[DBU-PEG]-[NTf_2], Silicalite-1/[DBU-PEG]-[NTf_2], ZIF-8/[Bmim][NTf_2], ZSM-5/[Bmim][NTf_2], Silicalite/[Bmim][NTf_2], [C_2OHmim][Lys]

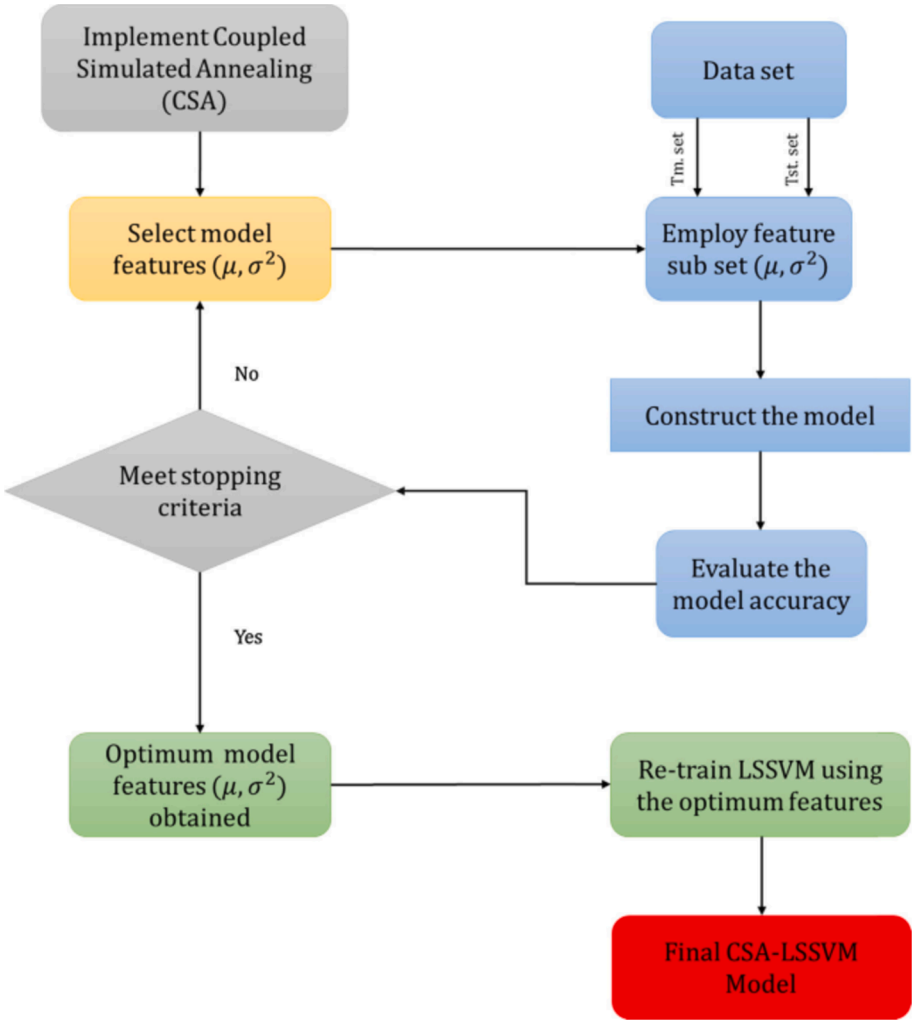

Fig. 2. Schematic of CSA-LSSVM algorithm [65] Copyright 2014, Reproduced with permission from Elsevier Science Ltd.

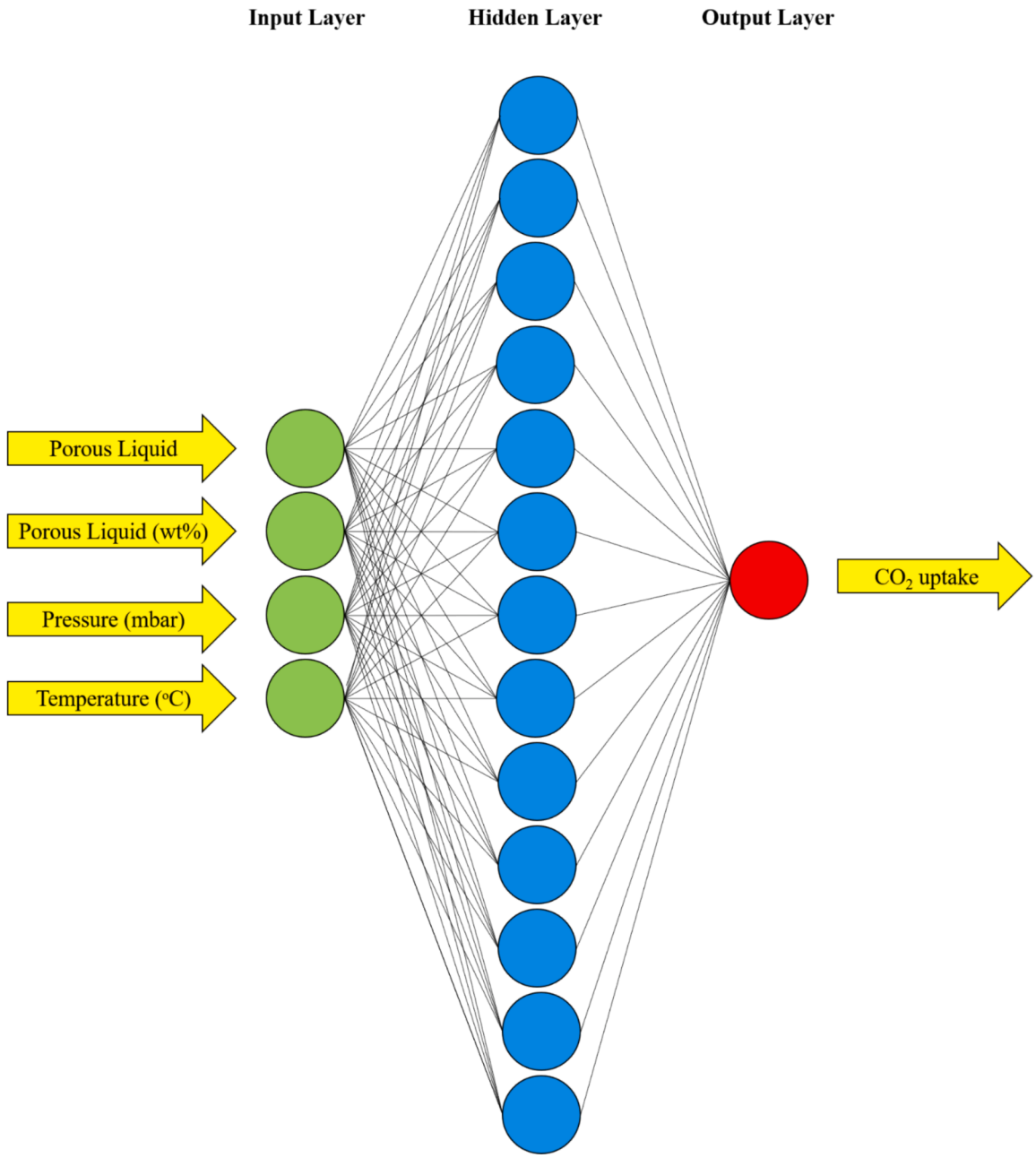

Fig. 3. Scheme of ANN structure in this study.

@GDX, and Al(fum)(OH)/PDMS. The PLs are identified by the names of the porous hosts and their percentage of mass in the porous liquids. For instance, PL No. 1 (Table 1) indicates that the host is ZIF-8, and its mass fraction in ZIF-8/[DBU-PEG]-[NTf_2] liquid nanocomposite is 3.2 %. The input parameters that were considered in these models are the PLs number which were denoted as 1 to 8 (Table 1), PLs wt%, temperature (T, °C), and pressure (P, mbar). In addition, two-dimensional or three-dimensional molecular descriptors can be used as inputs of the models for the identification of PL type, but they require additional complicated calculations based on Quantitative Structure-Property Relationship (QSPR). Such parameters can be explored in the modeling process in future. These 300 data points were used to develop a trustful approach to estimate CO_2 solubility in PL solvents. Of the total datasets, 75 % of the data were used as training and 25 % were used as testing data. The key factors that contribute to determining the CO_2 solubility are listed in Table 1.

4. Application of machine learning models

In this work, ANFIS, PSO-ANFIS, CSA-LSSVM, and MLP-NN with Levenberg Marquardt were utilized to estimate CO_2 solubility in the target PLs. By altering the neurons from 1 to 50, it was observed that the ANN structure with 13 neurons had the best accuracy and the lowest mean squared error (MSE). The MSE value for each neuron in predicting test and total data is represented in Table 2. The parameters of the optimum ANN model are provided in Table 3. The MSE The ANFIS model was developed based on Gaussian MF and genfis3 with six rules. An ANFIS model, enhanced by a PSO algorithm was used to assess the gas solubility in PLs. The PSO trained the Fuzzy C-means clustering (FCM) type ANFIS and determined the best values for the ANFIS parameters. These optimized values can be adjusted by different parametric studies to establish the PSO-ANFIS. The PSO task in the PSO–ANFIS model is to enhance the ANFIS to generate better connections between the input and the output. Moreover, as addressed in the literature, Gaussian type was

Table 1
Experimental data used in this study.

PL	PL No.	PL (wt %)	T (°C)	P (mbar)	CO_2 uptake (mmol/g)	Ref.
ZIF-8/[DBU-PEG]-[NTf_2]	1	3.2, 10, 20, 30	25	496.3–10000	0.016–1.56	[70]
ZSM-5/[DBU-PEG]-[NTf_2]	2	5.3	25	47.50–10000	0.011–0.46	
Silicalite-1/[DBU-PEG]-[NTf_2]	3	2.1	25	356.3–10000	0.009–0.38	
ZIF-8/[Bmim][NTf_2]	4	2.9	25	212.8–10000	0.013–0.66	
ZSM-5/[Bmim][NTf_2]	5	3.3	25	200.9–10000	0.013–0.62	
Silicalite/[Bmim][NTf_2]	6	2.9	25	82.74–10000	0.008–0.63	
[C_2OHmim][Lys]@GDX	7	30, 40, 55, 70, 80	40	0–1000	0.239–1.29	[71]
Al(fum)(OH)/PDMS	8	12.5	25–75	1000–5000	0.147–0.97	[72]

applied as MFs [73,74]. A trial-and-error process was used to evaluate the optimal values of the PSO parameters (Table 4). In this study, the suggested LSSVM model was integrated with CSA to achieve faster and more efficient convergence to optimal values. Employing this approach, the parameters σ^2 and γ were determined to be 0.6319 and 113197.34. The computation time for ANN, ANFIS, PSO-ANFIS and CSA-LSSVM was < 1 min, < 1 min, about 6 min, and < 1 min, respectively. For applying the models, MATLAB R2010b was used in Dell LATITUDE 5530, with 12th Gen – Intel® Core™ i7-1265U 1.8 GHz and 16 GB RAM.

5. Results and discussion

5.1. Accuracy of the developed models

Using the ML models developed in this work, CO_2 solubility in different PLs was calculated. Fig. 4 depicts the models' estimations versus the actual data point index to gain a realistic sense of model accuracy, and the result indicates a good fit between model results and real measurements. Fig. 5 shows the anticipated values in comparison with the target values for ANFIS, PSO-ANFIS, CSA-LSSVM, and MLP-NN models. Here, the horizontal and vertical axes are experimental and anticipated CO_2 solubility values in the tested PLs. The data points that are located close to isometric line show reliable estimation, and the anticipated values by all the developed models are acceptably close to the experimental data. Statistical parameters of MSE, R^2, AARD and standard deviation (STD) were applied, as shown in equations (20)-(23) to assess the integrity and accuracy of the models:

$$MSE = \frac{1}{n}\sum_{i=1}^{n}\left(x_i^{experimental} - x_i^{estimated}\right)^2 \tag{20}$$

$$R^2 = 1 - \frac{\sum_{i=1}^{n}\left[x_i^{estimated} - x_i^{experimental}\right]^2}{\sum_{i=1}^{n}\left[x_i^{estimated} - x^m\right]^2}, x_m = \frac{\sum_{i=1}^{n} x_i^{experimental}}{n} \tag{21}$$

$$AARD(\%) = \frac{100}{n}\sum_{i=1}^{n}\frac{\left|x_i^{estimated} - x_i^{experimental}\right|}{x_i^{experimental}} \tag{22}$$

$$\mathrm{STD} = \sqrt{\sum_{i=1}^{n}\left(\frac{\left(x_i^{estimated} - x_m\right)^2}{n}\right)} \tag{23}$$

where x_m is the average of experimental data, and n is the number of data.

The above parameters are widely used in regression analysis and prediction, and have been reported in many publications [43,75–78]. The results (Table 5) show that of the four models, the R^2 values are very high (≥ 0.94) while MSE values are very small (≤ 0.0041). However, CSA-LSSVM has the lowest %AARD for the total and test data. It can be concluded that all the developed models predicted the CO_2 solubility

Table 2
MSE of each neuron in ANN.

Test MSE	Neuron	Test MSE	Neuron	Total MSE	Neuron	Total MSE	Neuron
0.0561	1	0.0034	23	0.0679	1	0.0034	45
0.0365	2	0.0033	39	0.0379	2	0.0032	50
0.0195	48	0.0032	32	0.0117	31	0.0032	6
0.0126	3	0.0032	17	0.0111	3	0.0031	18
0.0102	31	0.0031	44	0.0100	12	0.0030	9
0.0096	12	0.0031	6	0.0098	48	0.0030	23
0.0074	37	0.0031	5	0.0097	16	0.0029	21
0.0073	16	0.0030	8	0.0071	32	0.0029	34
0.0058	41	0.0030	34	0.0066	37	0.0028	10
0.0052	33	0.0030	10	0.0053	4	0.0028	46
0.0052	50	0.0027	46	0.0051	36	0.0028	8
0.0050	42	0.0027	24	0.0050	42	0.0027	30
0.0049	28	0.0027	21	0.0050	25	0.0026	15
0.0048	29	0.0026	18	0.0045	29	0.0026	17
0.0045	25	0.0026	35	0.0043	7	0.0026	27
0.0045	4	0.0024	27	0.0041	33	0.0026	26
0.0043	19	0.0024	26	0.0038	41	0.0025	11
0.0042	14	0.0023	47	0.0038	44	0.0022	24
0.0041	20	0.0023	49	0.0037	19	0.0022	38
0.0041	7	0.0022	38	0.0037	14	0.0021	49
0.0037	40	0.0021	15	0.0036	28	0.0020	35
0.0036	11	0.0019	36	0.0036	40	0.0019	47
0.0035	9	0.0019	43	0.0035	20	0.0017	43
0.0035	45	0.0017	22	0.0035	5	0.0015	22
0.0035	30	0.0005	13	0.0034	39	0.0008	13

Table 3
The parameters of the optimum ANN model.

No. of neuron	Activation function	Training function	Input-to-hidden layer weights	Hidden-to-output layer weights	Input-to-hidden layer bias	Hidden-to-output layer bias
13	logsig	trainlm	−1.605407641	−2.398934285	4.667523302	−0.930436315
			−5.873688764	−4.791949484	3.388719217	
			4.206560575	−3.456662989	−5.904947868	
			0.407451586	−3.313063395	2.534438846	
			2.371211204	−2.672258534	2.976970477	
			−2.524364649	−5.23304348	−2.709247429	
			−3.107074887	2.037353588	−2.61480374	
			2.162605746	1.206215307	−1.194174788	
			2.015669156	−4.072891622	−2.36054217	
			−2.222918928	−1.276478957	−3.129859452	
			−5.169629449	3.065997794	−5.926180115	
			8.789907394	1.364055099	4.156422334	
			−0.496704753	13.29864177	41.43791644	

Table 4
Properties of the PSO-ANFIS model.

Variable	Value
Iterations	400
Particles	2500
Initial inertia weight	0.7
Inertia weight damping ratio	0.89
Cognitive acceleration (C_1)	1
Social acceleration (C_2)	2
Number of fuzzy rules	10

with high accuracy. In comparing the model performance between the training, validation and test datasets, better results were obtained in the training stage, except for the MLP-NN model. The MSE and R^2 values for the test set of the MLP-NN model are slightly better than the training dataset, which could be due to the randomness in dividing data and the model structure.

Table 6 show the value of %AARD of the estimated values by developed models obtained for each PL. The results show that CSA-LSSVM presented the lowest %AARD for all PLs except [C_2OHmim][Lys]@GDX in which MLP-NN presented the lowest %AARD for [C_2OHmim][Lys]@GDX. The results demonstrate that all models, especially CSA-LSSVM and ANN can be used for the estimation of CO_2 solubility in PLs at different temperatures, pressures and wt% of PLs. Therefore, these two models can be used for predicting CO_2 solubility in new PLs in future.

5.2. *Effects of input parameters on CO_2 absorption*

This part presents the intricacies of CO_2 adsorption and solubility in tested PLs, employing both experimental data and model results to understand the dynamics of gas capture. It also evaluates the efficacy of these PLs under different conditions, highlighting the role of PL wt%, ionic liquids, and polymer frameworks in enhancing CO_2 capture capabilities. Through a comparison of experimental results with results

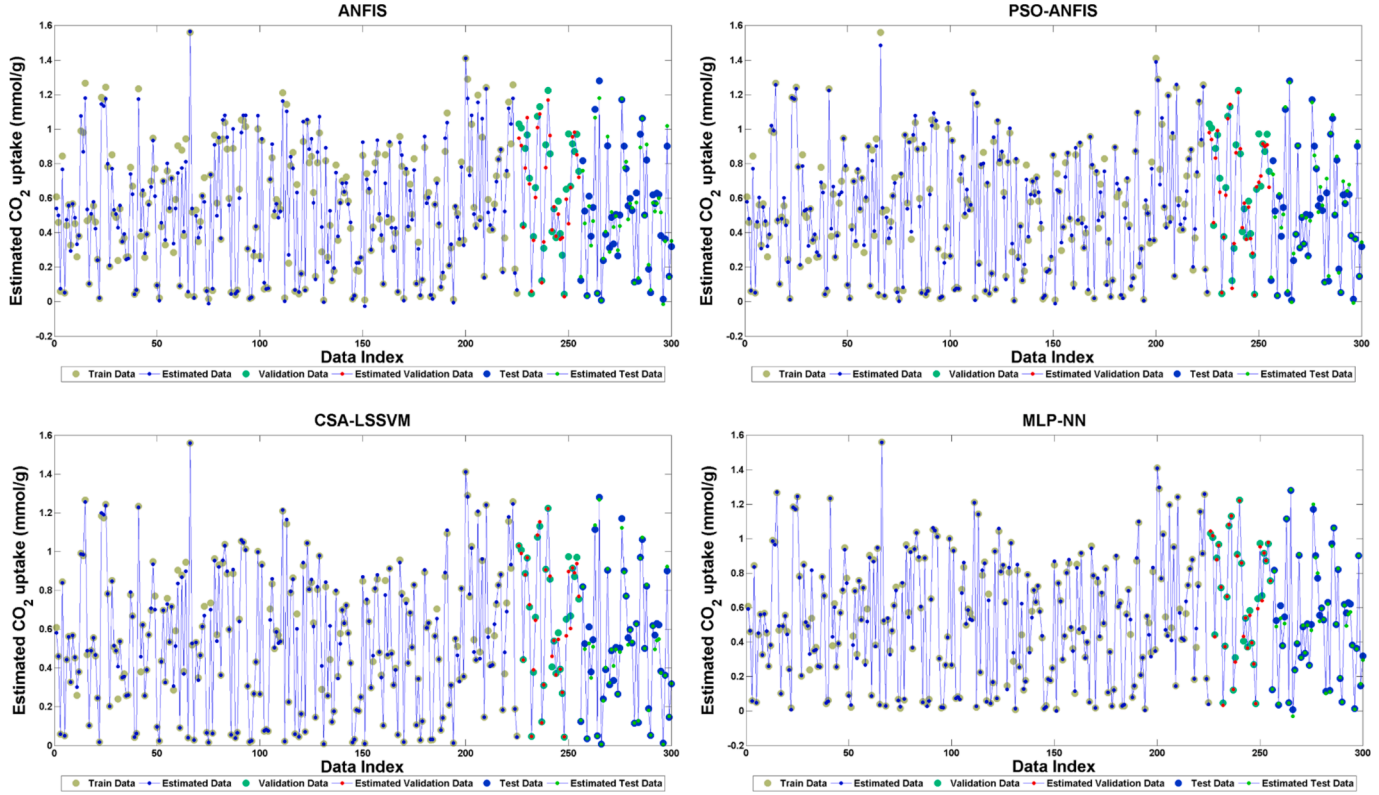

Fig. 4. Experimental CO_2 solubility versus estimated data at testing and training stages.

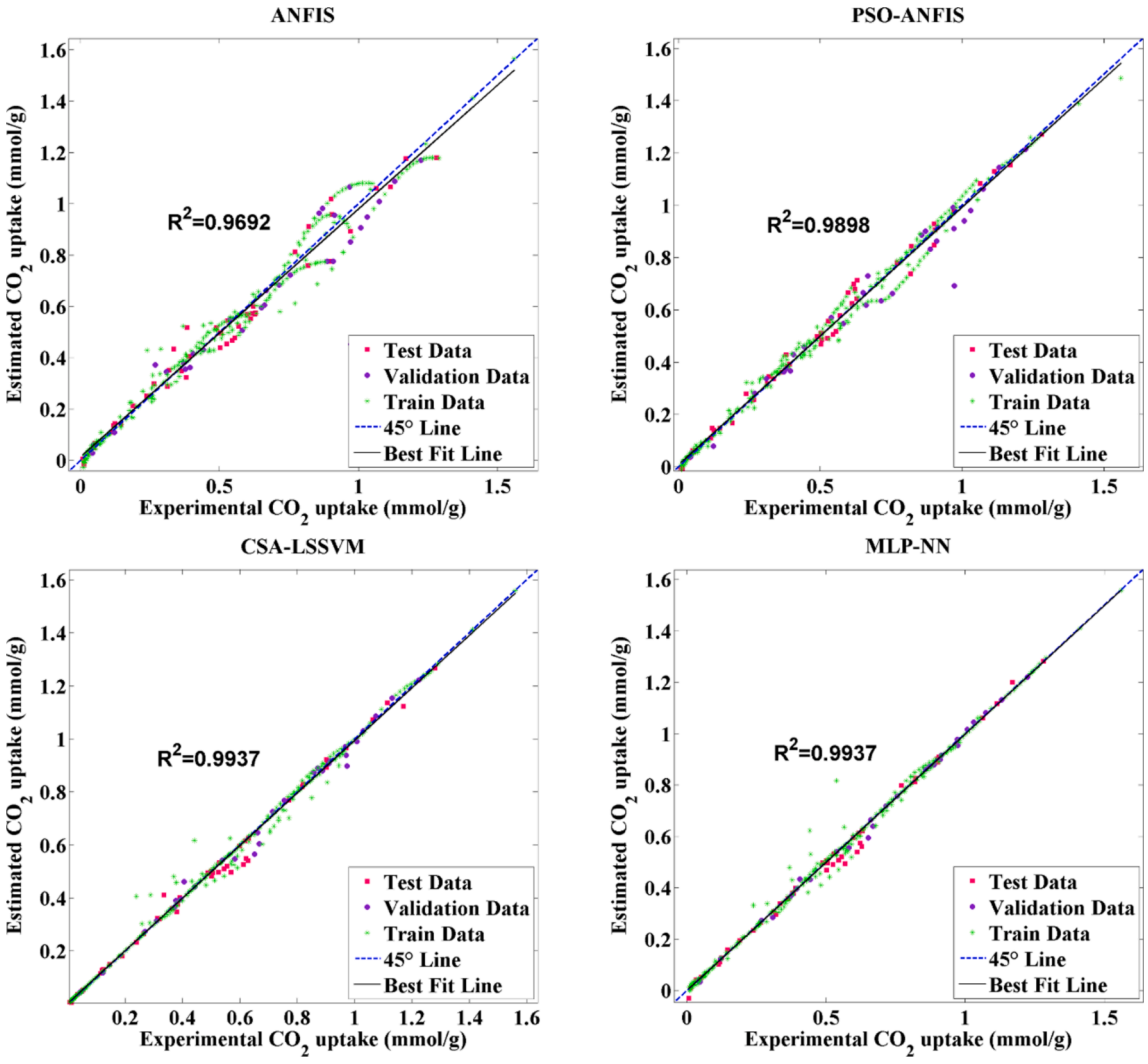

Fig. 5. Regression plots between the experimental and estimated CO_2 solubility.

Table 5
Statistical analyses result for the developed models.

Parameter	Train	Validation	Test	Total
ANFIS				
R^2	0.9790	0.8739	0.9715	0.9692
MSE	0.0026	0.0135	0.0030	0.0037
STD	0.3507	0.3132	0.3206	0.3444
% AARD	12.88	11.64	14.35	12.98
PSO-ANFIS				
R^2	0.9927	0.9610	0.9904	0.9898
MSE	0.0009	0.0041	0.001	0.0012
STD	0.3519	0.3179	0.3294	0.3472
% AARD	8.13	7.29	12.29	8.67
CSA-LSSVM				
R^2	0.9941	0.9922	0.9917	0.9937
MSE	0.0007	0.0008	0.0008	0.0007
STD	0.3531	0.3255	0.3258	0.3491
% AARD	2.79	2.92	5.26	3.17
MLP-NN				
R^2	0.9931	0.9977	0.9943	0.9937
MSE	0.0008	0.0002	0.0006	0.0007
STD	0.3553	0.3294	0.3307	0.3519
% AARD	5.49	2.81	14.94	6.64

from the computational models, insights are gleaned into the mechanisms driving CO_2 solubility and adsorption in these innovative materials. The exploration in this section underscores the potential of PLs in addressing environmental challenges and sets the stage for future research directions aimed at optimizing PLs for more efficient CO_2 capture, reflecting a significant step forward in the quest for sustainable environmental solutions.

Table 6
AARD (%) of the developed models for the estimation of CO_2 solubility in PLs.

PL	ANFIS	PSO-ANFIS	CSA-LSSVM	MLP-NN
ZIF-8/[DBU-PEG]-[NTf_2]	7.73	6.04	0.79	4.76
ZSM-5/[DBU-PEG]-[NTf_2]	40.71	23.35	2.29	15.85
Silicalite-1/[DBU-PEG]-[NTf_2]	29.39	13.96	3.53	8.47
ZIF-8/[Bmim][NTf_2]	32.30	24.89	5.52	6.41
ZSM-5/[Bmim][NTf_2]	19.98	19.17	1.62	7.91
Silicalite/[Bmim][NTf_2]	13.65	15.90	2.06	37.70
[C_2OHmim][Lys]@GDX	8.83	4.91	4.25	3.28
Al(fum)(OH)/PDMS	6.03	5.57	0.70	5.39

Fig. 6 is concerned with the comparison between model estimations and experimental data regarding the CO_2 adsorption capability of ZIF-8/[DBU-PEG]-[NTf_2] with 20 wt% at ambient temperature [70]. This comparison is crucial for the validation of the model's results against actual observed data. The enhancement of CO_2 capturing capacity, attributed to the high surface area and porosity of ZIF-8/[DBU-PEG]-[NTf_2] when incorporated into porous liquids, is demonstrated. The

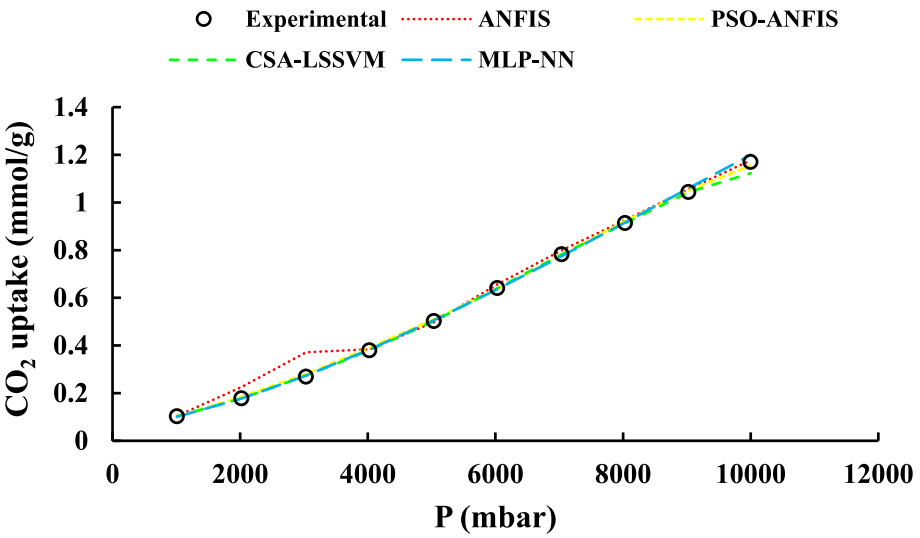

Fig. 6. Comparison of experimental and estimated CO_2 solubility in 20 wt% ZIF-8/[DBU-PEG]-[NTf_2] at ambient temperature.

effectiveness of the model in capturing the nuances of CO_2 adsorption behavior in these systems is highlighted along with the reliability of the model and the potential of ZIF-8/[DBU-PEG]-[NTf_2] in CO_2 capture applications [79]. Fig. 7 shows the comparison for CO_2 solubility in 12.5 wt% Al(fum)(OH)/PDMS under varied operational conditions [72]. The system of Al(fum)(OH)/PDMS, which combines a metal–organic framework with polydimethylsiloxane (a silicone type), is shown to have a specific affinity towards CO_2. The variations in operational conditions, which include temperature, pressure, and the presence of other gases, are seen to influence CO_2 solubility. The accuracy of the model across a spectrum of conditions is tested. The adaptability and efficiency of Al(fum)(OH)/PDMS as a medium for CO_2 solubility offer insights into its applications in gas separation technologies [80]. Fig. 8 focuses on the experimental and estimated CO_2 adsorption capacities in [C_2OHmim][Lys]@GDX with varying contents at 40 °C [71]. It assesses the model's ability to estimate CO_2 adsorption across different compositions of [C_2OHmim][Lys]@GDX, emphasizing the impact of chemical composition and concentration on CO_2 capture efficiency. [C_2OHmim][Lys]@GDX, a novel type of ionic liquid-based porous liquid, is shown where specific interactions between the ionic liquid and CO_2 are exploited to enhance CO_2 capture [81].

In order to evaluate the model performance, CO_2 solubility in different PLs at the same conditions is compared (Table 7). As the results show, at the pressure of 5000 mbar, 3 wt% of PL, and temperature of 25 °C, LSSVM predicted that ZSM-5/[Bmim][NTf_2] yields the highest CO_2 capture, and ANN predicted that Al(fum)(OH)/PDMS yields the

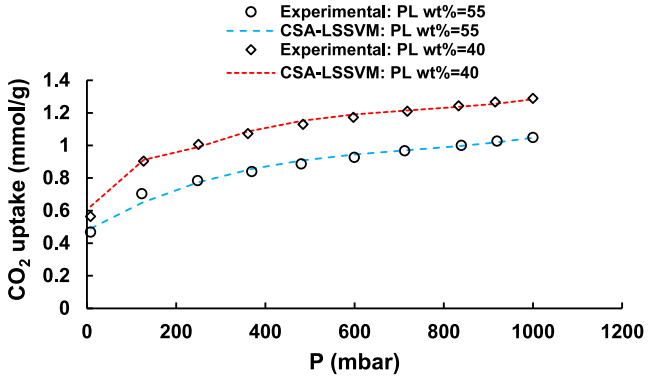

Fig. 8. Comparison of experimental and estimated CO_2 solubility of [C_2OHmim][Lys]@GDX with different wt% at 40 °C.

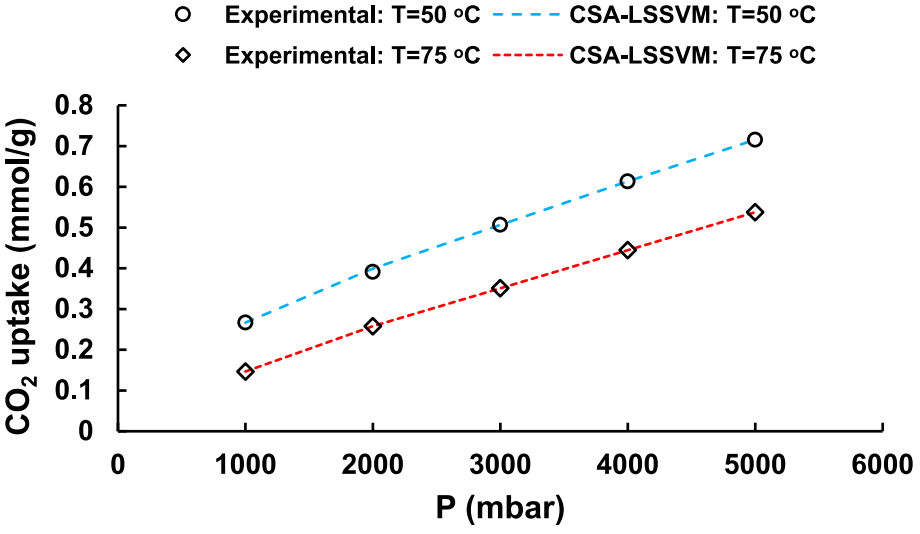

Fig. 7. Comparison of experimental and estimated CO_2 solubilities in 12.5 wt% Al(fum)(OH)/PDMS at different operational conditions.

highest value.

Collectively, these figures illustrate the innovative application of PLs in CO_2 capture technology, highlighting the complex relationship between material composition, operational conditions, and CO_2 adsorption/solubility. Through the comparison of experimental data with model estimations, the utility of models in guiding the development and optimization of new PLs for environmental applications is validated. These analyses contribute valuable insights into the design and application of PLs in addressing the crucial challenge of CO_2 capture and sequestration, marking a significant advancement in the field of sustainable environmental technologies.

6. Conclusions

In this study, a novel approach for estimating CO_2 solubility in various PLs is proposed, utilizing the ML models including ANFIS, PSO-ANFIS, MLP-NN, and CSA-LSSVM. CSA-LSSVM showed the best accuracy with the lowest ARRD value (3.17 %) compared to other models with AARD of 6.64 %, 8.67 % and 12.98 % for MLP-NN, PSO-ANFIS and ANFIS models. The findings indicate that CSA-LSSVM achieved the lowest AARD for all PLs except [C_2OHmim][Lys]@GDX for which MLP-NN recorded the lowest AARD. This research offers a reliable method for estimating CO_2 solubility in diverse PLs, providing researchers and practitioners with a practical tool that relies on minimal number of dependent parameters to estimate CO_2 absorption in PLs. Through this work, a significant advancement can be made in the field of CO_2 capture, by offering a reliable and efficient tool for the development of new PLs tailored for enhanced CO_2 absorption capabilities. The ML models developed here will support the researchers and industrialists to accurately predict CO_2 capture by PLs in various operational situations, to operate the CO_2 capture systems under optimized and desired conditions, and for advanced control of such systems. Therefore, such ML modeling tools provide guidance for CO_2 capture by new PLs in future. The accurate, efficient, and cost-effective models can be highly complementary for experimental measuring of CO_2 capture by PLs.

Declaration of generative AI in scientific writing

During the preparation of this work, the authors used Grammarly and ChatGPT to improve readability and language. After using this tool/service, the authors reviewed and edited the content as needed and take full responsibility for the content of the publication.

CRediT authorship contribution statement

Farid Amirkhani: Resources, Data curation, Visualization, Writing – review & editing. **Amir Dashti:** Methodology, Writing – review & editing, Software, Writing – original draft. **Hossein Abedsoltan:** Writing – original draft, Investigation. **Amir H. Mohammadi:** Conceptualization, Supervision, Writing – review & editing. **John L. Zhou:** Supervision, Writing – review & editing. **Ali Altaee:** Writing – review & editing.

Declaration of competing interest

The authors declare that they have no known competing financial interests or personal relationships that could have appeared to influence the work reported in this paper.

Appendix A. Supplementary material

Supplementary data to this article can be found online at https://doi.org/10.1016/j.seppur.2024.130445.

Table 7
Prediction of CO_2 solubility in different PLs at the same conditions (3 wt% PL, 25 °C, 500 mbar).

PL	ANFIS	PSO-ANFIS	CSA-LSSVM	MLP-NN
ZIF-8/[DBU-PEG]-[NTf_2]	0.2079	0.2121	0.1998	0.1961
ZSM-5/[DBU-PEG]-[NTf_2]	0.1619	0.0821	0.0667	0.0658
Silicalite-1/[DBU-PEG]-[NTf_2]	0.2433	0.2548	0.1034	0.2157
ZIF-8/[Bmim][NTf_2]	0.2967	0.3192	0.2840	0.3211
ZSM-5/[Bmim][NTf_2]	0.2982	0.3372	0.3122	0.3060
Silicalite/[Bmim][NTf_2]	0.2929	0.3331	0.3022	0.3073
[C_2OHmim][Lys]@GDX	0.2889	0.2000	0.0209	0.3862
Al(fum)(OH)/PDMS	0.2950	−0.6066	−0.1404	0.9083

Data availability

Data will be made available on request.

References

[1] S.N. Habisreutinger, L. Schmidt-Mende, J.K. Stolarczyk, Photocatalytic reduction of CO_2 on TiO2 and other semiconductors, Angew. Chem. Int. Ed. 52 (2013) 7372–7408.
[2] X. Chang, T. Wang, J. Gong, CO_2 photo-reduction: Insights into CO_2 activation and reaction on surfaces of photocatalysts, Energ. Environ. Sci. 9 (2016) 2177–2196.
[3] J. Ran, M. Jaroniec, S.Z. Qiao, Cocatalysts in semiconductor-based photocatalytic CO_2 reduction: Achievements, challenges, and opportunities, Adv. Mater. 30 (2018) 1704649.
[4] B. Stats, Statistical Review of World Energy 2020, Accessed, 11 (2020) 2020.
[5] U. Kamran, S.-J. Park, Chemically modified carbonaceous adsorbents for enhanced CO_2 capture: A review, J. Clean. Prod. 290 (2021) 125776.
[6] M. Asif, M. Suleman, I. Haq, S.A. Jamal, Post-combustion CO_2 capture with chemical absorption and hybrid system: Current status and challenges, Greenh. Gases Sci. Technol. 8 (2018) 998–1031.
[7] S. Choi, J.H. Drese, C.W. Jones, Adsorbent materials for carbon dioxide capture from large anthropogenic point sources, ChemSusChem: Chem. Sustain. Energy Mater. 2 (2009) 796–854.
[8] Y. Takamura, J. Aoki, S. Uchida, S. Narita, Application of high-pressure swing adsorption process for improvement of CO_2 recovery system from flue gas, Can. J. Chem. Eng. 79 (2001) 812–816.
[9] F. Amirkhani, M. Mosadegh, M. Asghari, M.J. Parnian, The beneficial impacts of functional groups of CNT on structure and gas separation properties of PEBA mixed matrix membranes, Polym. Test. 82 (2020) 106285.
[10] F. Amirkhani, H.R. Harami, M. Asghari, CO_2/CH_4 mixed gas separation using poly (ether-b-amide)-ZnO nanocomposite membranes: Experimental and molecular dynamics study, Polym. Test. 86 (2020) 106464.
[11] M. Mosadegh, F. Amirkhani, H.R. Harami, M. Asghari, M.J. Parnian, Effect of Nafion and APTEOS functionalization on mixed gas separation of PEBA-FAU membranes: Experimental study and MD and GCMC simulations, Sep. Purif. Technol. 247 (2020) 116981.
[12] R. Thiruvenkatachari, S. Su, H. An, X.X. Yu, Post combustion CO_2 capture by carbon fibre monolithic adsorbents, Prog. Energy Combust. Sci. 35 (2009) 438–455.
[13] M. Fang, N. Yi, W. Di, T. Wang, Q. Wang, Emission and control of flue gas pollutants in CO2 chemical absorption system–A review, Int. J. Greenh. Gas Control 93 (2020) 102904.
[14] A.K. Voice, G.T. Rochelle, Products and process variables in oxidation of monoethanolamine for CO_2 capture, Int. J. Greenh. Gas Control 12 (2013) 472–477.
[15] A. Pohorille, L.R. Pratt, Cavities in molecular liquids and the theory of hydrophobic solubilities, J. Am. Chem. Soc. 112 (1990) 5066–5074.
[16] X. Zhao, Y. Ding, L. Ma, X. Zhu, H. Wang, Q. Liao, An enhancement of CO_2 capture in a type-III porous liquid by 2-Methylimidazole zinc salt (ZIF-8), J. Mol. Liq. 367 (2022) 120523.
[17] A. Knebel, A. Bavykina, S.J. Datta, L. Sundermann, L. Garzon-Tovar, Y. Lebedev, S. Durini, R. Ahmad, S.M. Kozlov, G. Shterk, Solution processable metal–organic frameworks for mixed matrix membranes using porous liquids, Nat. Mater. 19 (2020) 1346–1353.
[18] G. Singh, J. Lee, A. Karakoti, R. Bahadur, J. Yi, D. Zhao, K. AlBahily, A. Vinu, Emerging trends in porous materials for CO_2 capture and conversion, Chem. Soc. Rev. 49 (2020) 4360–4404.
[19] K. Jie, N. Onishi, J.A. Schott, I. Popovs, D.e. Jiang, S. Mahurin, S. Dai, Transforming porous organic cages into porous ionic liquids via a supramolecular complexation strategy, Angewandte Chemie, 132 (2020) 2288-2292.
[20] C. Eaborn, Compendium of chemical Terminology: IUPAC Recommendations: compiled by V. Gold, KL Loening, AD McNaught, and P. Sehmi, Blackwell, Oxford, etc., 1987, viii+ 456 pages.£ 45.00 (hard cover) ISBN 0-632-01765-1;£ 29.50 (soft cover) ISBN 0-632-01767-3, in, Elsevier, 1988.

[21] P. Li, J.A. Schott, J. Zhang, S.M. Mahurin, Y. Sheng, Z.A. Qiao, X. Hu, G. Cui, D. Yao, S. Brown, Electrostatic-assisted liquefaction of porous carbons, Angew. Chem. 129 (2017) 15154–15158.

[22] Y. Xin, H. Ning, D. Wang, X. Li, W. Fan, X. Ju, H. Wang, Y. Zhang, Z. Yang, D. Yao, A generalizable strategy based on the rule of "like dissolves like" to construct porous liquids with low viscosity for CO_2 capture, Nano Res. 16 (2023) 10369–10380.

[23] J. Avila, L.F. Lepre, C.C. Santini, M. Tiano, S. Denis-Quanquin, K. Chung Szeto, A. A. Padua, M. Costa Gomes, High-performance porous ionic liquids for low-pressure CO_2 capture, Angew. Chem. 133 (2021) 12986–12992.

[24] B. Dutcher, M. Fan, A.G. Russell, Amine-based CO_2 capture technology development from the beginning of 2013: A Review, ACS Applied Materials & Interfaces, 7 (2015) 2137-2148.

[25] A. Eslamimanesh, F. Gharagheizi, A.H. Mohammadi, D. Richon, Artificial neural network modeling of solubility of supercritical carbon dioxide in 24 commonly used ionic liquids, Chem. Eng. Sci. 66 (2011) 3039–3044.

[26] H. Liu, J. Qu, A.H. Bhatti, F. Barzagli, C.e. Li, J. Bi, R. Zhang, A generic machine learning model for CO_2 equilibrium solubility into blended amine solutions, Separation and Purification Technology, 334 (2024) 126100.

[27] C. Mukesh, S. Sarmad, A. Samikannu, D. Nikjoo, W. Siljebo, J.-P. Mikkola, Pore size-excluded low viscous porous liquids for CO_2 sorption at room temperature and thermodynamic modeling study, J. Mol. Liq. 356 (2022) 119046.

[28] M. Atilhan, A. Cincotti, S. Aparicio, Nanoscopic characterization of type II porous liquid and its use for CO_2 absorption from molecular simulation, J. Mol. Liq. 330 (2021) 115660.

[29] M. Safamirzaei, H. Modarress, Application of neural network molecular modeling for correlating and predicting Henry's law constants of gases in [bmim][PF6] at low pressures, Fluid Phase Equilib. 332 (2012) 165–172.

[30] M.C. Kroon, E.K. Karakatsani, I.G. Economou, G.-J. Witkamp, C.J. Peters, Modeling of the carbon dioxide solubility in imidazolium-based ionic liquids with the tPC-PSAFT equation of state, J. Phys. Chem. B 110 (2006) 9262–9269.

[31] A. Rostami, M. Arabloo, H. Ebadi, Genetic programming (GP) approach for prediction of supercritical CO_2 thermal conductivity, Chem. Eng. Res. Des. 122 (2017) 164–175.

[32] C. Li, H. Liu, M. Xiao, X. Luo, H. Gao, Z. Liang, Thermodynamics and ANN models for predication of the equilibrium CO_2 solubility in aqueous 3-dimethylamino-1-propanol solution, Int. J. Greenh. Gas Control 63 (2017) 77–85.

[33] G. Chen, X. Luo, H. Zhang, K. Fu, Z. Liang, W. Rongwong, P. Tontiwachwuthikul, R. Idem, Artificial neural network models for the prediction of CO_2 solubility in aqueous amine solutions, Int. J. Greenh. Gas Control 39 (2015) 174–184.

[34] A. Tatar, A. Barati-Harooni, A. Najafi-Marghmaleki, A. Bahadori, Accurate prediction of CO_2 solubility in eutectic mixture of levulinic acid (or furfuryl alcohol) and choline chloride, Int. J. Greenh. Gas Control 58 (2017) 212–222.

[35] M.M. Ghiasi, A.H. Mohammadi, Rigorous modeling of CO_2 equilibrium absorption in MEA, DEA, and TEA aqueous solutions, J. Nat. Gas Sci. Eng. 18 (2014) 39–46.

[36] J.-S. Jang, C.-T. Sun, Neuro-fuzzy modeling and control, Proc. IEEE 83 (1995) 378–406.

[37] A. Dashti, A. Bahrololoomi, F. Amirkhani, A.H. Mohammadi, Estimation of CO_2 adsorption in high capacity metal− organic frameworks: Applications to greenhouse gas control, J. CO_2 Util. 41 (2020) 101256.

[38] A. Dashti, M. Jokar, F. Amirkhani, A.H. Mohammadi, Quantitative structure property relationship schemes for estimation of autoignition temperatures of organic compounds, J. Mol. Liq. 300 (2020) 111797.

[39] A. Baghban, M. Bahadori, J. Rozyn, M. Lee, A. Abbas, A. Bahadori, A. Rahimali, Estimation of air dew point temperature using computational intelligence schemes, Appl. Therm. Eng. 93 (2016) 1043–1052.

[40] K. Ahangari, S.R. Moeinossadat, D. Behnia, Estimation of tunnelling-induced settlement by modern intelligent methods, Soils Found. 55 (2015) 737–748.

[41] J.-S.-R. Jang, C.-T. Sun, E. Mizutani, Neuro-fuzzy and soft computing-a computational approach to learning and machine intelligence [Book Review], IEEE Trans. Autom. Control 42 (1997) 1482–1484.

[42] J.-S. Jang, ANFIS: Adaptive-network-based fuzzy inference system, IEEE Trans. Syst. Man Cybern. 23 (1993) 665–685.

[43] S.A. Hoseinpour, A. Barati-Harooni, P. Nadali, A. Mohebbi, A. Najafi-Marghmaleki, A. Tatar, A. Bahadori, Accurate model based on artificial intelligence for prediction of carbon dioxide solubility in aqueous tetra-n-butylammonium bromide solutions, J. Chemom. 32 (2018) e2956.

[44] B.K. Panigrahi, Y. Shi, M.-H. Lim, Handbook of swarm intelligence: concepts, principles and applications, Springer Science & Business Media, 2011.

[45] J. Kennedy, R. Eberhart, Particle swarm optimization (PSO), in: Proc. IEEE International Conference on Neural Networks, Perth, Australia, 1995, pp. 1942-1948.

[46] Y. Shi, R.C. Eberhart, Empirical study of particle swarm optimization, in: Proceedings of the 1999 Congress on Evolutionary Computation-CEC99 (Cat. No. 99TH8406), IEEE, 1999, pp. 1945-1950.

[47] M. Clerc, The swarm and the queen: towards a deterministic and adaptive particle swarm optimization, in: Proceedings of the 1999 congress on evolutionary computation-CEC99 (Cat. No. 99TH8406), IEEE, 1999, pp. 1951-1957.

[48] F. Amirkhani, A. Dashti, H. Abedsoltan, A.H. Mohammadi, A.G. Chofreh, F.A. Goni, J.J. Klemeš, Estimating flashpoints of fuels and chemical compounds using hybrid machine-learning techniques, Fuel 323 (2022) 124292.

[49] V. Vapnik, The nature of statistical learning theory, Springer Science & Business Media, 1999.

[50] V. Vapnik, Statistical Learning Theory, Wiley-Interscience, New York, 1998.

[51] T. Van Gestel, J. De Brabanter, B. De Moor, J. Vandewalle, J. Suykens, T. Van Gestel, Least Squares Support Vector Machines, 2002.

[52] Y. Wang, S. Zhang, Z. Liu, H. Li, L. Wang, Characterization and expression of AmphiCL encoding cathepsin L proteinase from amphioxus Branchiostoma belcheri tsingtauense, Mar. Biotechnol. 7 (2005) 279–286.

[53] S.P. Mousavi, S. Atashrouz, M. Nait Amar, A. Hemmati-Sarapardeh, A. Mohaddespour, A. Mosavi, Viscosity of ionic liquids: Application of the Eyring's theory and a committee machine intelligent system, Molecules 26 (2020) 156.

[54] F. Zeng, M. Nait Amar, A.S. Mohammed, M.R. Motahari, M. Hasanipanah, Improving the performance of LSSVM model in predicting the safety factor for circular failure slope through optimization algorithms, Eng. Comput. (2021) 1–12.

[55] M. Cai, O. Hocine, A.S. Mohammed, X. Chen, M.N. Amar, M. Hasanipanah, Integrating the LSSVM and RBFNN models with three optimization algorithms to predict the soil liquefaction potential, Eng. Comput. 38 (2022) 3611–3623.

[56] S. Kirkpatrick, C.D. Gelatt Jr, M.P. Vecchi, Optimization by simulated annealing, Science 220 (1983) 671–680.

[57] H. Safari, A. Shokrollahi, M. Jamialahmadi, M.H. Ghazanfari, A. Bahadori, S. Zendehboudi, Prediction of the aqueous solubility of $BaSO_4$ using pitzer ion interaction model and LSSVM algorithm, Fluid Phase Equilib. 374 (2014) 48–62.

[58] H.R. Holakoei, F. Sajedi, Compressive strength prediction of SLWC using RBFNN and LSSVM approaches, Neural Comput. & Applic. 35 (2023) 6685–6697.

[59] A. Dashti, A.H. Navidpour, F. Amirkhani, J.L. Zhou, A. Altaee, Application of machine learning models to improve the prediction of pesticide photodegradation in water by ZnO-based photocatalysts, Chemosphere 362 (2024) 142792.

[60] F. Amirkhani, A. Dashti, M. Jokar, A.H. Mohammadi, A.G. Chofreh, P.S. Varbanov, J.L. Zhou, Estimation of CO_2 solubility in aqueous solutions of commonly used blended amines: Application to optimised greenhouse gas capture, J. Clean. Prod. 430 (2023) 139435.

[61] F. Amirkhani, A. Dashti, H. Abedsoltan, A.H. Mohammadi, Estimation of CO_2 Absorption by a Hybrid Aqueous Solution of Amino Acid Salt with Amine, Chem. Eng. Technol. 47 (2024) 253–261.

[62] A. Dashti, F. Amirkhani, A.-S. Hamedi, A.H. Mohammadi, Evaluation of CO_2 absorption by amino acid salt aqueous solution using hybrid soft computing methods, ACS Omega 6 (2021) 12459–12469.

[63] J.A. Suykens, J. Vandewalle, B. De Moor, Intelligence and cooperative search by coupled local minimizers, Int. J. Bifurcation Chaos 11 (2001) 2133–2144.

[64] S. Xavier-de-Souza, J.A. Suykens, J. Vandewalle, D. Bollé, Coupled simulated annealing, IEEE Trans. Syst. Man Cybernetics Part B (Cybernetics) 40 (2009) 320–335.

[65] M. Mesbah, E. Soroush, V. Azari, M. Lee, A. Bahadori, S. Habibnia, Vapor liquid equilibrium prediction of carbon dioxide and hydrocarbon systems using LSSVM algorithm, J. Supercrit. Fluids 97 (2015) 256–267.

[66] A.H. Mohammadi, D. Richon, Use of artificial neural networks for estimating water content of natural gases, Ind. Eng. Chem. Res. 46 (2007) 1431–1438.

[67] M. Lashkarbolooki, A.Z. Hezave, S. Ayatollahi, Artificial neural network as an applicable tool to predict the binary heat capacity of mixtures containing ionic liquids, Fluid Phase Equilib. 324 (2012) 102–107.

[68] M.A. Sedghamiz, A. Rasoolzadeh, M.R. Rahimpour, The ability of artificial neural network in prediction of the acid gases solubility in different ionic liquids, J. CO_2 Util. 9 (2015) 39–47.

[69] M. Lashkarbolooki, B. Vaferi, M. Rahimpour, Comparison the capability of artificial neural network (ANN) and EOS for prediction of solid solubilities in supercritical carbon dioxide, Fluid Phase Equilib. 308 (2011) 35–43.

[70] W. Shan, P.F. Fulvio, L. Kong, J.A. Schott, C.-L. Do-Thanh, T. Tian, X. Hu, S. M. Mahurin, H. Xing, S. Dai, New class of type III porous liquids: A promising platform for rational adjustment of gas sorption behavior, ACS Appl. Mater. Interfaces 10 (2018) 32–36.

[71] J. Wu, Z. Yang, J. Xie, P. Zhu, J. Wei, R. Jin, H. Yang, Porous polymer supported amino functionalized ionic liquid for effective CO_2 capture, Langmuir 39 (2023) 2729–2738.

[72] J. Cahir, M.Y. Tsang, B. Lai, D. Hughes, M.A. Alam, J. Jacquemin, D. Rooney, S. L. James, Type 3 porous liquids based on non-ionic liquid phases–A broad and tailorable platform of selective, fluid gas sorbents, Chem. Sci. 11 (2020) 2077–2084.

[73] M. Raji, A. Dashti, P. Amani, A.H. Mohammadi, Efficient estimation of CO_2 solubility in aqueous salt solutions, J. Mol. Liq. 283 (2019) 804–815.

[74] A. Dashti, M. Raji, A. Razmi, N. Rezaei, S. Zendehboudi, M. Asghari, Efficient hybrid modeling of CO_2 absorption in aqueous solution of piperazine: Applications to energy and environment, Chem. Eng. Res. Des. 144 (2019) 405–417.

[75] F. Amirkhani, A. Dashti, H. Abedsoltan, A.H. Mohammadi, K.-W. Chau, Towards estimating absorption of major air pollutant gasses in ionic liquids using soft computing methods, J. Taiwan Inst. Chem. Eng. 127 (2021) 109–118.

[76] A. Dashti, O. Mazaheri, F. Amirkhani, A.H. Mohammadi, Molecular descriptors-based models for estimating net heat of combustion of chemical compounds, Energy 217 (2021) 119292.

[77] A. Dashti, F. Amirkhani, M. Jokar, A. Mohammadi, K.-W. Chau, Insights into the estimation of heavy metals ions sorption from aqueous environment onto natural zeolite, Int. J. Environ. Sci. Technol. 18 (2021) 1773–1784.

[78] A. Rostami, A. Baghban, S. Shirazian, On the evaluation of density of ionic liquids: towards a comparative study, Chem. Eng. Res. Des. 147 (2019) 648–663.

[79] G. Jin, H. Wang, K. Zhang, H. Zhang, J. Fan, J. Wang, D. Guo, Z. Wang, ZIF-8 based porous liquids with high hydrothermal stability for carbon capture, Mater. Today Commun. 36 (2023) 106820.

[80] J. Avila, R. Clark, A.A. Pádua, M.C. Gomes, Porous ionic liquids: beyond the bounds of free volume in a fluid phase, Mater. Adv. 3 (2022) 8848–8863.

[81] Z. Xu, T. Wang, J. Wu, L. Wang, X. Zhang, H. Dong, C. Sun, Mass transfer characteristics of CO2 and blended aqueous solutions of [C2OHmim][Lys]/MDEA in a microchannel, Ind. Eng. Chem. Res. (2023).